

Accuracy of direct gradient sensing by single cells

Robert G. Endres^{1,2,3} and Ned S. Wingreen¹

¹*Department of Molecular Biology, Princeton University,
Princeton, NJ 08544-1014, USA*

²*Division of Molecular Biosciences,
Imperial College London,
London SW7 2AZ, United Kingdom*

³*Centre for Integrated Systems Biology at Imperial College,
Imperial College London,
London SW7 2AZ, United Kingdom*

Many types of cells are able to accurately sense shallow gradients of chemicals across their diameters, allowing the cells to move towards or away from chemical sources. This chemotactic ability relies on the remarkable capacity of cells to infer gradients from particles randomly arriving at cell-surface receptors by diffusion. Whereas the physical limits of concentration sensing by cells have been explored, there is no theory for the physical limits of gradient sensing. Here, we derive such a theory, using as models a perfectly absorbing sphere and a perfectly monitoring sphere, which, respectively, infer gradients from the absorbed surface particle density or the positions of freely diffusing particles inside a spherical volume. We find that the perfectly absorbing sphere is superior to the perfectly monitoring sphere, both for concentration and gradient sensing, since previously observed particles are never remeasured. The superiority of the absorbing sphere helps explain the presence at the surfaces of cells of signal degrading enzymes, such as PDE for cAMP in *Dictyostelium discoideum* (Dicty) and BAR1 for mating factor α in *Saccharomyces cerevisiae* (budding yeast). Quantitatively, our theory compares favorably to recent measurements of Dicty moving up a cAMP gradient, suggesting these cells operate near the physical limits of gradient detection.

Cells are able to sense gradients of chemical concentration with extremely high sensitivity. This is done either directly, by measuring spatial gradients across the cell diameter, or indirectly, by temporally sensing gradients while moving. In temporal sensing, a cell modifies its swimming behavior according to whether a chemical concentration is rising or falling in time [1]. This mode of sensing is typical of small, fast moving bacteria such as *Escherichia coli*, which can respond to changes in concentration as low as 3.2 nM of the attractant aspartate [2]. In contrast, direct spatial sensing is prevalent among larger, single-celled eukaryotic organisms such as the slime mold *Dictyostelium discoideum* (Dicty) and the yeast *Saccharomyces cerevisiae* [3, 4]. Dicty cells are able to sense a concentration difference of only 1-5% across the cell [5], corresponding to a difference in receptor occupancy between front and back of only 5 receptors [6]. Spatial sensing is also performed with high accuracy by cells of the immune system including neutrophils and lymphocytes [7], as well as by growing synaptic cells and tumor cells. While there has been great progress in understanding the limits of concentration sensing and signaling in bacteria such as *E. coli* [8, 9, 10, 11, 12, 13], very little is known about the theoretical limits of direct gradient sensing by eukaryotic cells.

In a recent set of experiments, van Haastert and Postma [6] measured the Chemotactic Index of Dicty cells in a cAMP gradient (Fig. 1, symbols). Chemotactic Index is defined as the distance moved in the direction of the cAMP gradient divided by the total distance moved. To obtain the data in Fig. 1, van Haastert and Postma used a pipette containing different concen-

trations of cAMP. Diffusion of cAMP out of the pipette established a steady-state cAMP gradient, with magnitude a function of distance from the pipette. Chemotaxis was observed for cells as far as 700 μ m from a pipette filled with 10^{-4} M cAMP, corresponding to a mean concentration of 7 nM and a gradient of only 0.01 nM/ μ m. This remarkable chemotactic ability raises the question – how closely does gradient sensing by Dicty cells compare with the fundamental limits on gradient sensing set by diffusion?

Here we derive the fundamental limits of gradient sensing using two models for cells: a perfectly absorbing sphere and a perfectly monitoring sphere. Within the theory, gradients are estimated by comparing the discrete positions of particles, either absorbed on the surface of the sphere or measured inside the spherical volume, with the expected continuous distribution originating from a particular gradient. We find that a perfectly absorbing sphere is superior to a perfectly monitoring sphere for sensing both concentrations and gradients (Table I), since previously observed particles are never remeasured. Quantitatively, our theory (Fig. 1, solid curves) compares favorably with recent measurements of Dicty cells migrating to a cAMP-filled pipette [6], suggesting that chemotactic ability of Dicty approaches the fundamental limits set by diffusion.

I. LIMITS OF CONCENTRATION SENSING

In this section, we consider the limits of concentration sensing set by particle diffusion. Consider as a measure-

ment device a spherical cell of radius a that can measure the local concentration of a certain dissolved chemical. Such an idealized device may make measurements following two different strategies: (1) The device can either act as a *perfectly absorbing sphere* and record the number of absorbed particles on its surface or (2) act as a *perfectly monitoring sphere* and count the number of particles inside its volume. In either case, from the number of particles, an estimate of the chemical concentration can be obtained. However, these estimates have an intrinsic uncertainty due to the randomness of particle diffusion.

Perfectly Absorbing Sphere. For the perfectly absorbing sphere the uncertainty in measuring a background chemical concentration c is straightforward to derive. At steady state, the average particle current impinging on the sphere is $J = 4\pi Dac$, where D is the chemical diffusion constant. The average number of particles absorbed in time T is $N = 4\pi DacT$. Since the particles are independent, N is Poisson distributed, *i.e.* $\langle(\delta N)^2\rangle = \langle N \rangle$. Therefore, the perfectly absorbing sphere has a concentration-measurement uncertainty of

$$\frac{\langle(\delta c)^2\rangle}{c^2} = \frac{\langle(\delta N)^2\rangle}{\langle N \rangle^2} = \frac{1}{4\pi DacT}. \quad (1)$$

Perfectly Monitoring Sphere. The perfectly monitoring sphere was introduced by Berg and Purcell [8] as a parameter-free model for a cell that "perfectly" binds and releases all ligands that contact its surface. To quantify the time a diffusing particle spends in the cell's vicinity and is therefore capable of being measured, Berg and Purcell treated the cell as a permeable sphere that infers the particle concentration by counting the number of particles N inside its volume, and improves accuracy by averaging over several statistically independent measurements. A simple estimate for the resulting uncertainty in concentration can be obtained as follows: the number N is Poisson distributed and the cell counts approximately $N = a^3 c$ particles in its volume at any time. During a time T , the cell can make $N_{\text{meas}} = T/(a^2/D)$ independent measurements, where a^2/D is the typical turnover time for particles inside the sphere, leading to

$$\frac{\langle(\delta c)^2\rangle}{c^2} = \frac{\langle(\delta N)^2\rangle}{N^2} = \frac{1}{N_{\text{meas}} N} \approx \frac{1}{Dact}. \quad (2)$$

Berg and Purcell [8] derived the exact concentration-measurement uncertainty for a perfectly monitoring sphere ("perfect instrument") from the time correlations of particles inside the sphere, and obtained

$$\frac{\langle(\delta c)^2\rangle}{c^2} = \frac{3}{5\pi DacT}, \quad (3)$$

which is identical to the estimate in Eq. 2 up to a nu-

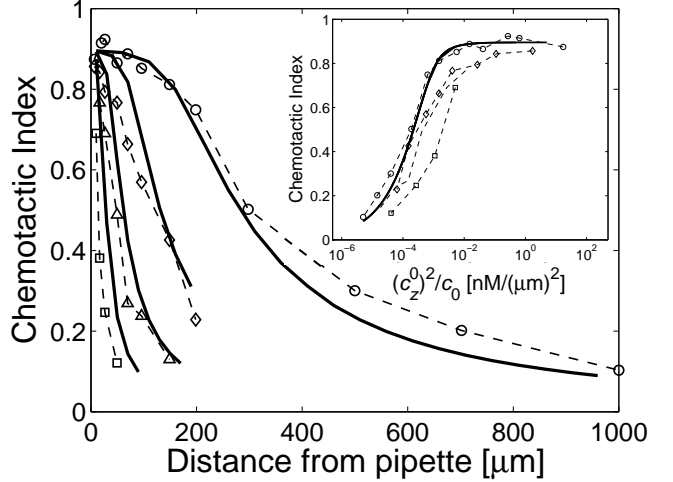


FIG. 1: Comparison between the Chemotactic Index determined by experiment (symbols and dashed lines) and our theory (solid curves). Chemotactic Index is defined as the distance moved by a cell in the direction of a gradient divided by the total distance moved. Experimental data was obtained by van Haastert and Postma [6] from *Dictyostelium discoideum* cells migrating toward pipettes containing four different cAMP concentrations, 0.1 μM (squares), 1 μM (triangles), 10 μM (diamonds), 100 μM (circles). The theoretical curves were obtained for a perfectly absorbing sphere using a single fitting parameter $Da^3T = 1.2 \cdot 10^5 \mu\text{m}^5$, corresponding to, *e.g.*, a cAMP diffusion constant of $D = 300 \mu\text{m}^2/\text{s}$, a cell radius of $a = 5 \mu\text{m}$, and an averaging time $T = 3.2 \text{ s}$, using the gradient profiles from Ref. [6] and the Chemotactic Index from Eq. 21. Experimentally, the Chemotactic Index only reaches approximately 0.9 at zero distance, so we rescale our theory curves by 0.9. Inset: Chemotactic Index as a function of $(c_z^0)^2/c_0$ in units of $\text{nM}/(\mu\text{m})^2$, where c_z^0 and c_0 are the gradient and concentration, respectively.

merical prefactor.

However, notice that the concentration-measurement uncertainty of the perfectly absorbing sphere is actually *smaller* than that of a perfectly monitoring sphere of the same size, because the perfectly absorbing sphere removes particles from the environment, and hence does not measure the same particle more than once.

II. LIMITS OF GRADIENT SENSING

Now consider the *perfectly absorbing sphere* and the *perfectly monitoring sphere* as devices for measuring the local gradient of a certain dissolved chemical. In both cases, measurements of discrete particles can be compared with the expected continuous distribution of particles originating from a particular gradient (Fig. 2a), and hence, the gradient can be estimated. Here, we present in brief a theoretical derivation of the intrinsic uncertainty of gradient sensing (for details see supporting information). We find that the intrinsic uncertainty

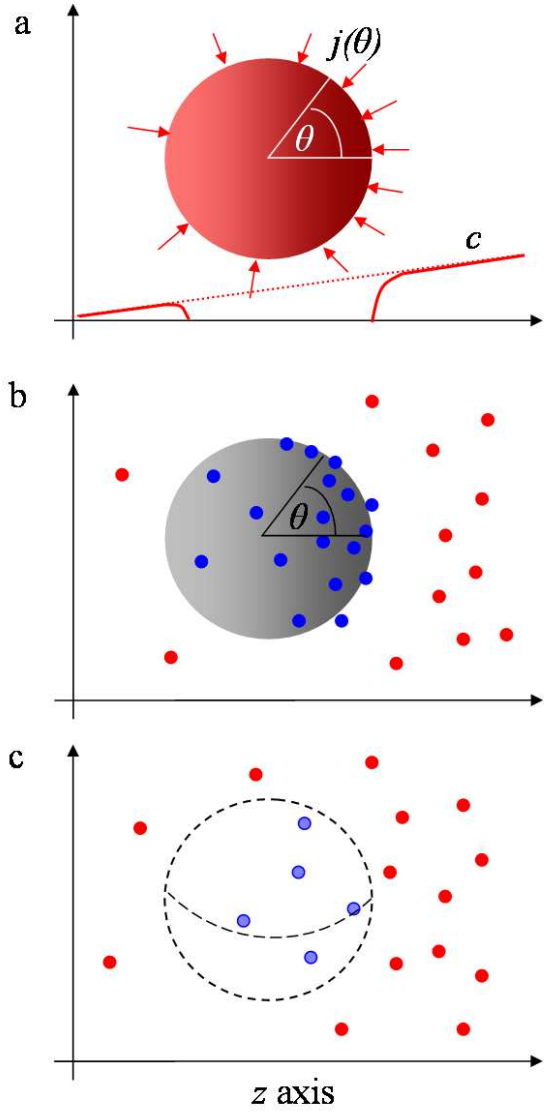


FIG. 2: Idealized models for gradient sensing by a cell. The gradient points along the z -axis, which is shown horizontally. (a) Continuum model for a perfectly absorbing sphere. The mean particle current density $j(\theta)$ impinging on the sphere has axial symmetry; θ measures the angle with respect to the z -axis. At steady-state, the particle concentration c is zero immediately outside the perfectly absorbing sphere, as shown schematically by the red curve superposed on the dotted background gradient. (b) Discrete particle model for the perfectly absorbing sphere. From the number and positions of particles absorbed during time T , the background particle concentration and gradient can be estimated. (c) Perfectly monitoring sphere. Particles diffuse in and out of the sphere without resistance. By monitoring, for a time T , the number and positions of particles inside the sphere, the background concentration and gradient can be estimated.

is independent of the actual gradient present, and is always much smaller (by a factor of $7/60 \simeq 12\%$) for the perfectly absorbing sphere.

Perfectly Absorbing Sphere. The average particle current density $\vec{j} = -D\vec{\nabla}c$ impinging on the surface of a perfectly absorbing sphere of radius a at steady state follows from the diffusion equation, $\nabla^2c = 0$, and is given in polar coordinates by

$$j(\theta, \phi) = \frac{Dc_0}{a} + 3D\vec{c}_r \cdot \vec{e}(\theta, \phi), \quad (4)$$

where c_0 is a constant background concentration, \vec{c}_r is the background gradient, and $\vec{e}(\theta, \phi) = (\cos\phi\sin\theta, \sin\phi\sin\theta, \cos\theta)$ is a unit vector normal to the surface of the sphere (see Fig. 2a). To best estimate the chemical gradient from an observed discrete density of particles absorbed at the surface of the sphere during time T (Fig. 2b), requires fitting the observed density $\sigma_T^{\text{obs}} = \sum_{i=1}^N \delta(\vec{r} - \vec{r}_i)$, where N is the total number of absorbed particles, to the expected density $j(\theta, \phi)T$ from Eq. 4. Since the estimates of the components of the gradient in the x , y , and z directions are independent, without loss of generality, we consider only the gradient estimate in the z -direction, *i.e.* $c_z = \partial c / \partial z$, and later generalize to an arbitrary gradient. From the best fit, the estimate for the gradient in the z -direction after absorption of particles for a time T is given by

$$c_z = \frac{\int \sigma_T^{\text{obs}} \cos\theta dA}{4\pi Da^2 T} = \frac{\sum_{i=1}^N \cos\theta_i}{4\pi Da^2 T}, \quad (5)$$

where θ_i is the polar angle of the i th absorbed particle. We are interested in the uncertainty (accuracy) of the gradient measurement, which is given by the variance

$$\begin{aligned} \langle (\delta c_z)^2 \rangle &= \langle c_z^2 \rangle - \langle c_z \rangle^2 \quad (6) \\ &= \frac{\langle \sum_{i=1}^N \cos^2 \theta_i \rangle + \langle \sum_{i=1}^N \sum_{i \neq j} \cos \theta_i \cos \theta_j \rangle}{(4\pi Da^2 T)^2} \\ &\quad - \frac{\langle \sum_{i=1}^N \cos \theta_i \rangle^2}{(4\pi Da^2 T)^2} \\ &= \frac{\langle \sum_{i=1}^N \cos^2 \theta_i \rangle}{(4\pi Da^2 T)^2} = \frac{\langle N \rangle \langle \cos^2 \theta \rangle}{(4\pi Da^2 T)^2} = \frac{c_0}{12\pi Da^3 T}. \end{aligned}$$

The derivation of Eq. 6 made use of the independence of the particles to factorize the expectation value as $\langle \sum_{i=1}^N \sum_{i \neq j} \cos \theta_i \cos \theta_j \rangle = \langle N(N-1) \rangle \langle \cos \theta \rangle^2 = \langle N \rangle^2 \langle \cos \theta \rangle^2$, since the number of absorbed particles N is Poisson distributed. We also used $\langle N \rangle = 4\pi Da c_0 T$, as well as $\langle \cos^2 \theta \rangle = 1/3$. (The relation $\langle \cos^2 \theta_i \rangle = \langle \cos^2 \theta \rangle$ for absorbed particles holds even in the presence of a true gradient in the z direction since the gradient-weighted contribution $\langle \cos^3 \theta \rangle$ is zero.)

In three dimensions, the total uncertainty of the gra-

dient, normalized by c_0/a , is given by

$$\frac{\langle(\delta c_{\vec{r}})^2\rangle}{(c_0/a)^2} = \frac{3\langle(\delta c_z)^2\rangle}{(c_0/a)^2} = \frac{1}{4\pi D a c_0 T}, \quad (7)$$

with the factor of 3 arising because each component of the gradient contributes independently to the total uncertainty. This result for the uncertainty in gradient sensing is independent of the magnitude of the actual gradient present, including the case when no actual gradient is present. Curiously, the result is numerically identical to the concentration-measurement uncertainty (Eq. 1).

Perfectly Monitoring Sphere.

Here, we extend Berg and Purcell's analysis of the perfectly monitoring sphere ("perfect instrument") to include gradient sensing. Specifically, we assume that the monitoring sphere measures not only the number but also the positions of all particles in its volume (Fig. 2c). The best estimate of the gradient is obtained by fitting a concentration gradient with a $c = c_0 + \vec{c}_r \cdot \vec{r}$ to the observed time-averaged number density $\frac{1}{T} \int dt \rho_{\text{obs}}(t) = \frac{1}{T} \int dt \sum_{i=1}^N \delta(\vec{r} - \vec{r}_i(t))$, obtained by measuring the exact positions of all the particles inside the volume of the sphere for a time T . As above we focus on one component of the gradient, namely the gradient in the z -direction c_z , and obtain as a best estimate

$$c_z = \frac{\frac{1}{T} \int dt \int dV z \rho_{\text{obs}}(t)}{\int dV z^2}, \quad (8)$$

where the integral $\int dV$ is over the volume of the sphere. We are interested in the variance of this estimated gradient

$$\begin{aligned} \langle(\delta c_z)^2\rangle &= \langle c_z^2 \rangle - \langle c_z \rangle^2 \\ &= \left(\frac{15}{4\pi a^5} \right)^2 [\langle m_{z,T}^2 \rangle - \langle m_{z,T} \rangle^2], \end{aligned} \quad (9)$$

where we have used $\int dV z^2 = 4\pi a^5/15$ and have defined

$$m_{z,T} = \frac{1}{T} \int dt \int dV z \rho_{\text{obs}}(t), \quad (10)$$

namely $m_{z,T}$ is the time-averaged total z -coordinate of particles inside the sphere. The expectation values in Eq.

9 are therefore given by

$$\begin{aligned} \langle m_{z,T}^2 \rangle &= \frac{1}{T^2} \left\langle \left(\int dt \int dV z \rho_{\text{obs}}(t) \right)^2 \right\rangle \quad (11) \\ &= \frac{1}{T^2} \int_0^T dt \int_0^T dt' \langle m_z(t) m_z(t') \rangle, \\ \langle m_{z,T} \rangle &= \frac{1}{T} \left\langle \left(\int dt \int dV z \rho_{\text{obs}}(t) \right) \right\rangle \\ &= \frac{1}{T} \int_0^T dt \langle m_z(t) \rangle, \end{aligned}$$

where the quantity $m_z(t)$ is the total of the z -coordinates of all the particles inside the sphere at time t . To calculate $m_z(t)$, we consider the sphere embedded inside a much larger volume containing a total of M particles. Then, $m_z(t) = \sum_{i=1}^M z_i(t)$, where z_i is the z -coordinate of particle i if this particle is inside the sphere and is zero otherwise. On average there will be $\langle N \rangle = \frac{4}{3}\pi a^3 c_0$ particles inside the sphere at any time t . The auto-correlation function $\langle m_z(t) m_z(t') \rangle$ of particles inside the sphere at time t and time t' can consequently be calculated as

$$\begin{aligned} \langle m_z(t) m_z(t') \rangle &= \left\langle \sum_{i=1}^M \sum_{j=1}^M z_i(t) z_j(t') \right\rangle \quad (12) \\ &= \frac{4}{3}\pi a^3 c_0 u(t - t') + \langle m_z(t) \rangle^2, \end{aligned}$$

where we have defined $u(t - t') = \langle z(t) z(t') \rangle$ for a single particle. Substituting Eqs. 11 and 12 into Eq. 9 results in

$$\langle(\delta c_z)^2\rangle = \frac{75c_0}{4\pi a^7 T^2} \int_0^T dt \int_0^T dt' u_0(t - t'). \quad (13)$$

By defining a correlation time $\tau_z = (1/a^2) \int_0^\infty d\tau u(\tau)$ for the coordinate $z(t)$, the double time integral in Eq. 13 can be simplified, provided the time T is much larger than τ_z . Using time-reversal symmetry $u(\tau) = u(-\tau)$ for equilibrium diffusion (assuming small gradients), the variance simplifies to

$$\langle(\delta c_z)^2\rangle = \frac{75c_0 \tau_z}{2\pi a^5 T}. \quad (14)$$

The remaining task is to calculate τ_z , the probability that a particle with coordinate z inside the sphere at time $t = 0$ is still (or again) inside the sphere at a later time τ . We first consider the case in which the background chemical concentration is uniform, and later consider the presence of an actual gradient. Based on the solution of the diffusion equation in three dimensions, if a unit amount of chemical is released at point \vec{r}' , the concentration at point \vec{r} at a later time τ is given by

$$f(|\vec{r} - \vec{r}'|, \tau) = \frac{\exp\left(-\frac{|\vec{r} - \vec{r}'|^2}{4D\tau}\right)}{(4\pi D\tau)^{\frac{3}{2}}}. \quad (15)$$

Using the result for the time integral from Ref. [8],

$$\int_0^\infty d\tau f(|\vec{r} - \vec{r}'|, \tau) = \frac{1}{4\pi D|\vec{r} - \vec{r}'|}, \quad (16)$$

the correlation time τ_z can be expressed as a volume integral over the sphere (the initial coordinate \vec{r}' is uniform in the sphere because we assume a uniform background chemical concentration)

$$\begin{aligned} \tau_z &= \frac{1}{\frac{4}{3}\pi a^5} \int_0^\infty d\tau \int dV z \int dV' z' f(|\vec{r} - \vec{r}'|, \tau) \quad (17) \\ &= \frac{3}{16\pi^2 D a^5} \int dV z \int dV' \frac{z'}{|\vec{r} - \vec{r}'|} \\ &= \frac{3}{16\pi^2 D a^5} \int dV z \psi(r, \theta), \end{aligned}$$

where $r = |\vec{r}|$. The function

$$\psi(r, \theta) = \int dV' \frac{z'}{|\vec{r} - \vec{r}'|} = \int dV' \frac{r' \cos \theta'}{|\vec{r} - \vec{r}'|} \quad (18)$$

is analogous to the potential of a charge density in electrostatics, specifically the charge density $\rho(z') = z' = \rho(r', \theta') = r' \cos \theta'$ for $r' \leq a$ and $\rho(r') = 0$ for $r' > a$. To solve the final integral in Eq. 17, we perform a multipole expansion of $\psi(r, \theta)$ in terms of Legendre polynomials $P_l(\cos \theta)$, exploiting the rotational symmetry of $\psi(r, \theta)$ about the z axis [14], leading to

$$\tau_z = \frac{2a^2}{105D}. \quad (19)$$

Now consider the contribution from an additional gradient with zero mean over the volume of the sphere. We need to perform the integrals over a non-uniform distribution in Eq. 17. Since a gradient along the z -axis contributes a factor $\cos \theta$, which leads to the vanishing integral $\int_0^\pi \sin \theta \cos^3 \theta d\theta = 0$, we conclude that only the constant background contributes to the uncertainty in the gradient measurement. Therefore, Eq. 19 for τ_z remains true even when an actual gradient is present.

The result for τ_z in Eq. 19 can be used in Eq. 14 to obtain the normalized uncertainty of gradient measurement by the perfectly monitoring sphere

$$\frac{\langle (\delta c_{\vec{r}})^2 \rangle}{(c_0/a)^2} = \frac{3\langle (\delta c_z)^2 \rangle}{(c_0/a)^2} = \frac{15}{7\pi D a c_0 T}, \quad (20)$$

where all three components of the gradient contribute independently. Hence, the perfectly monitoring sphere is not only inferior to the perfectly absorbing sphere for concentration sensing by a factor of $12/5$ in variance (cf. Eqs. 1 and 3), but is also inferior by an even larger factor of $60/7$ for gradient sensing (cf. Eq. 7).

III. COMPARISON WITH EXPERIMENT

Van Haastert and Postma [6] recently measured the Chemotactic Index of Dicty cells in a cAMP gradient [6] (Fig. 1, symbols). They used a pipette containing different concentrations of cAMP to establish a distance-dependent steady-state cAMP gradients. The Chemotactic Index was defined as the distance moved by the cell in the direction of the cAMP gradient divided by the total distance moved. How does the observed chemotactic ability of Dicty compare with the fundamental limits on gradient sensing set by diffusion? To facilitate comparison to the results of van Haastert and Postma [6], we have calculated the optimal Chemotactic Index for a cell acting as a perfectly absorbing sphere.

To obtain the optimal Chemotactic Index CI , we assume that after averaging for a time T , a cell moves at a constant velocity in the direction of the estimated gradient. If we take the actual gradient to point in the z -direction, then the chemotactic index for one run i is simply $\cos \theta_i$, where θ_i is the angle between the true gradient and the estimated gradient. If the velocity and run time are the same for each run, leading to a constant run length l , then the average Chemotactic Index is given by

$$CI = \frac{\sum_i^N l_z}{\sum_i^N l} = \frac{l \sum_i^N \cos \theta_i}{Nl} = \langle \cos \theta_i \rangle. \quad (21)$$

To evaluate $\langle \cos \theta_i \rangle$ for a perfectly absorbing sphere, we use our result (Eq. 7) for the variance of the estimated gradient in each direction, e.g. $\langle (\delta c_{x,y,z})^2 \rangle = c_0/(12\pi D a^3 T)$. Assuming a Gaussian distribution with these variances, as well as an actual gradient with mean value c_z^0 in the z direction, the 2-dimensional distribution of estimated gradients $c_{\vec{r}} = (c_x, c_z)$ is given by

$$P_{c_z}(c_x, c_z) = \frac{1}{2\pi\sigma_x\sigma_z} e^{-c_x^2/(2\sigma_x^2) - (c_z - c_z^0)^2/(2\sigma_z^2)}, \quad (22)$$

where $\sigma_{x,z} = \sqrt{\langle (\delta c_{x,z})^2 \rangle}$. From this distribution, we can obtain the optimal Chemotactic Index

$$\begin{aligned} CI &= \langle \cos \theta \rangle = \langle c_z / \sqrt{c_x^2 + c_z^2} \rangle \\ &= \sqrt{\frac{\pi y}{2}} e^{-y} [I_0(y) + I_1(y)], \end{aligned} \quad (23)$$

where $y = (c_z^0)^2/(4\sigma_z^2)$ and $I_{0(1)}$ is the first (second) order modified Bessel function of the first kind. Fig. 1 shows a comparison of the optimal CI (solid curves) with the data of Ref. [6]. Importantly, the comparison relies on only a single global fitting parameter representing gradient-sensing ability, namely the product $D a^3 T$ where D is the diffusion constant, a is the cell diameter, and T is the averaging time. Based on the estimates $D = 300 \mu\text{m}^2/\text{s}$ and $a = 5 \mu\text{m}$ [6], the averaging time is predicted to be about $T = 3.2$ s. (The perfect-monitor model yields an identical curve, but with a longer inferred averaging time

Measurement uncertainty	Perfect absorber	Perfect monitor	Ratio absorber/monitor
Concentration: $\frac{\langle (\delta c)^2 \rangle}{c_0^2}$	$\frac{1}{4\pi D a c_0 T}$ [8]	$\frac{3}{5\pi D a c_0 T}$	$\frac{12}{5} = 2.4$
Gradient: $\frac{\langle (\delta c_r)^2 \rangle}{(c_0/a)^2}$	$\frac{1}{4\pi D a c_0 T}$	$\frac{15}{7\pi D a c_0 T}$	$\frac{60}{7} \approx 8.6$

TABLE I: Uncertainties in measured concentration and concentration gradient for two idealized cell models: a perfectly absorbing sphere (second column) and a perfectly monitoring sphere (third column). Also provided is the ratio of the uncertainties of the absorber and monitor. Parameters: diffusion constant D , radius of sphere a , averaging time T , and average chemical concentration c_0 .

$T = 27.5$ s.) The theory for the optimal Chemotactic Index matches the experiment rather well. Eq. 23 further predicts that the Chemotactic Index depends on the gradient c_z^0 and the concentration c_0 only through the combination $(c_z^0)^2/c_0$ (Fig. 1, inset). Intuitively, $\sqrt{(c_z^0)^2/c_0}$ measures the signal to noise ratio - the signal is proportional to the true gradient $|c_z^0|$, while the noise from particle diffusion scales as $\sqrt{c_0}$. More generally, the optimal Chemotactic Index depends on all variables only through the combination $(c_z^0)^2 D a^3 T / c_0$. Moreover, the theory predicts the full distribution of run angles (see inset of Fig. S1 in supporting information), which can be obtained by integrating Eq. 22 in the radial direction for each angle θ .

IV. DISCUSSION

Many types of cells are known to measure spatial chemical gradients directly with high accuracy. In particular, *Dictyostelium discoideum* (Dicty) is well known to measure extremely shallow cAMP gradients important for fruiting body formation [3, 5, 6] and *Saccharomyces cerevisiae* (budding yeast) detects shallow gradients of α mating pheromone [15]. Accurate spatial sensing is also performed by cells of the immune system including neutrophils and lymphocytes [7]. The question arises what are the fundamental limits of gradient sensing set by chemical diffusion? Here we derived such limits using as model cells a perfectly absorbing sphere and a perfectly monitoring sphere [8]. Within the theory, gradients are estimated by comparing the discrete distribution of observed locations of particles, either absorbed on the surface of the sphere (Fig. 2b) or measured inside the sphere (Fig. 2c), with the expected continuous distribution originating from a gradient (Fig. 2a). We find that a perfectly absorbing sphere is superior to a perfectly monitoring sphere for concentration and gradient sensing by respective factors of 12/5 (= 2.4) and 60/7 (≈ 8.6) (Table I), since the perfectly absorbing sphere prevents rebinding of already measured particles. Indeed, the results presented here for the perfectly absorbing sphere represent the true fundamental limits of both concentration and gradient sensing by cells. Our theory for the limits of gradient sensing compares favorably with recent measurements by van Haastert and Postma [6] of Dicty cells migrating to a cAMP-filled pipette (Fig. 1), suggesting that Dicty chemotaxis approaches the fundamental limits

set by cAMP diffusion.

The marked superiority of the perfect absorber for concentration and gradient sensing leads us to conjecture that cells may have developed mechanisms to absorb ligands so as to prevent their rebinding. Such absorption could be implemented by ligand or ligand-receptor internalization or by degradation of bound ligands. Even degradation of ligands without measurement could be advantageous. For example, a perfect absorber that measures only a fraction f of incident particles has the same uncertainties given in Table I but with an effective measurement time $T_{\text{eff}} = fT$. Such an absorbing cell that measures only 12% of absorbed particles can still measure gradients as accurately as a perfectly monitoring sphere. Similarly, an absorbing sphere of radius a with two small measurement patches at its poles of radius s ($s \ll a$), *i.e.* with a measuring surface-area fraction $s^2/(2a^2)$, effectively reduces the averaging time for pole-to-pole gradients to $3s^2T/(2a^2)$ (supporting information). Consequently, a measuring surface fraction as small as 4% yields the same uncertainty as the monitoring sphere.

In fact, there are numerous examples in biology of ligand-receptor internalization [16] and ligand degradation on cell surfaces, which we speculate, might be related to gradient sensing. (1) Although many G-protein-coupled receptors are internalized by endocytosis [17], the cAMP receptor cAR1 in Dicty is not [18]. However, Dicty produces two forms of cyclic nucleotide phosphodiesterase (PDE), which degrade external cAMP [19, 20, 21]. One form is membrane-bound (mPDE) and effectively turns Dicty into an absorber, whereas the other form is soluble (ePDE). The membrane-bound form mPDE only accumulates during cell aggregation, supporting the idea that degradation of cAMP at the membrane helps accurate gradient sensing and navigation. Indeed, cells lacking mPDE display cell-autonomous chemotaxis defects even in mixed aggregates with isogenic wild-type cells [21]. Interestingly, there is good evidence that Dicty cells do carry out G-protein-coupled receptor mediated endocytosis of folic acid, another major Dicty chemoattractant [22]. (2) In budding yeast, the receptor Ste2 binds α -factor pheromone, initiating a mating response including directed growth (“shmooing”) towards a potential mating partner. Ligand-bound Ste2 undergoes internalization by endocytosis [23]. Furthermore, the protease Bar1 degrades α pheromone externally [24, 25], and may be largely membrane associated

[26]. (3) There are many examples of ligand-receptor internalization in developmental biology. For example, primordial germ cells in zebrafish migrate towards the chemokine SDF-1a that activates the receptor CXCR4b. Ligand-induced CXCR4b internalization is required for precise arrival of germ cells at their target destination [27]. These examples suggest a correlation between ligand internalization/degradation and the accuracy of cell polarization and movement. In presenting these admittedly speculative examples, our hope is to raise interest, across fields, in how the constraints of gradient-sensing accuracy may have shaped cellular sensing systems.

While the absorption of ligands can improve gradient sensing, there is an inherent problem for an absorbing cell to measure a gradient while moving. An absorbing cell moving in a uniform concentration creates an apparent gradient due to an increased flux of incoming particles at its front and a decreased flux of particles at its back [8]. Using the model of a spherical cell, the ratio of fluxes between front and back hemispheres is given by

$$R = 1 + \frac{3av_0}{D}, \quad (24)$$

where v_0 is the cell velocity, a is the cell radius, and D is the particle diffusion constant. On the other hand, the flux ratio of a stationary spherical cell in a gradient $|\vec{\nabla}c|$ with uniform background concentration c_0 is given by

$$R = 1 + \frac{3a|\vec{\nabla}c|}{c_0}. \quad (25)$$

Hence, a moving cell sees an apparent gradient

$$|\vec{\nabla}c| = \frac{v_0 c_0}{D}. \quad (26)$$

As an example, chemotaxis of Dicty to cAMP is observed at a mean concentration of 7nM in a gradient of only 0.01 nM/ μm [6]. A Dicty cell moving with a typical speed of 0.2 $\mu\text{m}/\text{s}$ at the same mean concentration but without a gradient creates an apparent gradient of about half the real gradient. There are several ways out of this dilemma. (1) Cells could separate measurement from movement at low gradients, *e.g.* by stopping, measuring the gradient, and then moving. Dicty would only need to stop for about $a^2/D \approx 0.1\text{s}$ based on cell radius of $a = 5\mu\text{m}$ and diffusion constant $D = 300\mu\text{m}^2/\text{s}$. (2) Cells could sense gradients transverse to their direction of motion. This is particularly advantageous for fast moving cells (*e.g.* bacteria) for which the apparent gradient can become more than 100 times steeper than the actual gradient [8]. (Indeed, the oxygen-sensing marine bacterium *Thiovulum majus* directly senses gradients transverse to its direction of motion [29].) Interestingly, Dicty cells moving on agar in the absence of a gradient appear to combine these two strategies. Qualitatively, the tips of elongated moving cells slow down and flatten, often producing two or

more distinct pseudopods. Cells then elongate and move (\sim one cell length) in the direction of one of the pseudopods before the process is repeated (Liang Li and Ted Cox, personal communication). By this strategy, Dicty may avoid locking onto a false, movement-generated gradient. (3) In principle, cells could compensate for the apparent motion-generated gradient, either by internal signal processing or by external chemical secretion. In fact, Dicty cells do secrete cAMP, primarily from their trailing edge during movement [4], but this cAMP secretion serves dominantly to facilitate cell aggregation, including cells following cells during streaming. Given the complex role of cAMP in Dicty aggregation, studies of Dicty chemotaxis using gradients of folate, which is absorbed [22] but apparently not secreted by Dicty, may ultimately prove simpler to interpret.

Our models of the absorbing and the monitoring spheres neglect all biochemical reactions, such as particle-receptor binding and downstream signaling, which could significantly increase measurement uncertainty beyond the fundamental limits described here. To study the effects of particle-receptor binding, we extended a formalism for the uncertainty of concentration sensing, recently developed by Bialek and Setayeshgar [10], to gradient sensing. We found that the measurement uncertainty allowing ligand rebinding is larger than the measurement uncertainty without rebinding, confirming the superiority of the absorber over the monitor (details will be published elsewhere). A number of mechanistic models for gradient sensing and chemotaxis have addressed the important questions of cell polarization, signal amplification, and adaptation [30, 31, 32, 33, 34, 35, 36], cell movement of individual cells [37, 38], cell aggregation with cAMP degradation by PDE [39], as well as sensing of fluctuating concentrations [10, 40, 41]. Our results on the fundamental limits of gradient sensing complement these models, and may ultimately help lead to a comprehensive description of eukaryotic chemotaxis [42].

Finally, we remark that the experiments by van Haastert and Postma used stationary spatial gradients [6]. Cells in such gradients might profit from remembering their direction of motion [43], and evidence for such internal memory was recently obtained [28, 44, 45]. It therefore might prove interesting to measure the chemotactic index for randomly changing gradients, to find out if cells indeed use their memory to improve chemotaxis.

Acknowledgments

We thank Naama Barkai, John Bonner, Rob Cooper, Ted Cox, Liang Li, Trudi Schupbach, Stanislas Shvartsman, and Monika Skoge for helpful suggestions. Both authors acknowledge funding from the Human Frontier Science Program (HFSP). RGE acknowledges funding from the Biotechnology and Biological Sciences Research Council grant BB/G000131/1 and the Centre for Integrated Systems Biology at Imperial College (CISBIC),

NSW acknowledges funding from National Science Foun-

dation grant PHY-0650617.

[1] Berg HC (1999) Motile behavior of bacteria. *Physics Today* 53: 24-29.

[2] Mao H, Cremer PS, Manson MD (2003) A sensitive versatile microfluidic assay for bacterial chemotaxis. *Proc Natl Acad Sci USA* 100: 5449-5454.

[3] Arkowitz RA (1999) Responding to attraction: chemotaxis and chemotropism in *Dictyostelium* and yeast. *Trends Cell Biol* 9: 20-37.

[4] Manahan CL, Iglesias PA, Long Y, Devreotes PN (2004) Chemoattractant signaling in *dictyostelium discoideum*. *Annu Rev Cell Dev Biol* 20:223-53.

[5] Mato JM, Losada A, Nanjundiah V, Konijn TM (1975) Signal input for a chemotactic response in the cellular slime mold *Dictyostelium discoideum*. *Proc Natl Acad Sci USA* 72: 4991-4993.

[6] van Haastert PJM, Postma M (2007) Biased random walk by stochastic fluctuations of chemoattractant-receptor interactions at the lower limit of detection. *Biophys J* 93: 1787-1796.

[7] Zigmond SH (1977) Ability of polymorphonuclear leukocytes to orient in gradients of chemotactic factors. *J Cell Biol* 75: 606-616

[8] Berg HC, Purcell EM (1977) Physics of chemoreception. *Biophys J* 20: 193-219.

[9] Bray D, Levin MD, Morton-Firth CJ (1998) Receptor clustering as a cellular mechanism to control sensitivity. *Nature* 393: 85-88.

[10] Bialek W, Setayeshgar S (2005) Physical limits to biochemical signaling. *Proc Natl Acad Sci USA* 102: 10040-10045.

[11] Mello BA, Tu Y (2005) An allosteric model for heterogeneous receptor complexes: understanding bacterial chemotaxis responses to multiple stimuli. *Proc Natl Acad Sci USA* 102: 17354-17359.

[12] Keymer JE, Endres RG, Skoge M, Meir Y, Wingreen NS (2006) Chemosensing in *Escherichia coli*: two regimes of two-state receptors. *Proc Natl Acad Sci USA* 103: 1786-1791.

[13] Endres RG, Wingreen NS (2006) Precise adaptation in bacterial chemotaxis through "assistance neighborhoods". *Proc Natl Acad Sci USA* 103: 13040-13044.

[14] Jackson JD (1975) *Classical Electrodynamics* (2nd Ed., Wiley, NewYork), Ch. 4.4.

[15] Segall JE (1993) Polarization of yeast cells in spatial gradients of α mating factor. *Proc Natl Acad Sci USA* 90: 8332-8336.

[16] Mukherjee S, Ghosh RN, Maxfield FR (1997) Endocytosis. *Physiol Rev* 77:759-803.

[17] Ferguson SS (2001) Evolving concepts in G protein-coupled receptor endocytosis: the role in receptor desensitization and signaling. *Pharmacol Rev* 53: 1-24.

[18] Caterina MJ, Hereld D, Devreotes PN (1995) Occupancy of the *Dictyostelium* cAMP receptor, cAR1, induces a reduction in affinity which depends upon COOH-terminal serine residues. *J Biol Chem* 270: 4418-4423.

[19] Malchow D, Ngele B, Schwarz H, Gerisch G (1972) Membrane-bound cyclic AMP phosphodiesterase in chemotactically responding cells of *Dictyostelium discoideum*. *Eur J Biochem* 28: 136-142.

[20] Shapiro RI, Franke J, Luna EJ, Kessin RH (1983) A comparison of the membrane-bound and extracellular cyclic AMP phosphodiesterases of *Dictyostelium discoideum*. *Biochim Biophys Acta* 785: 49-57.

[21] Sucgang R, Weijer CJ, Siegert F, Franke J, Kessin RH (1997) Null mutations of the *Dictyostelium* cyclic nucleotide phosphodiesterase gene block chemotactic cell movement in developing aggregates. *Dev Biol* 192: 181-192.

[22] Rifkin JL (2001) Folate reception by vegetative *Dictyostelium discoideum* amoebae: distribution of receptors and trafficking of ligand. *Cell Motil Cytoskeleton* 48: 121-129.

[23] Schandl KA, Jenness DD (1994) Direct evidence for ligand-induced internalization of the yeast α -factor pheromone receptor. *Mol Cell Biol* 14: 7245-7255.

[24] Hicks JB, Herskowitz I (1976) Evidence for a new diffusible element of mating pheromones in yeast. *Nature* 260: 246-248.

[25] Barkai N, Rose MD, Wingreen NS (1998) Protease helps yeast find mating partners. *Nature* 396: 422-423.

[26] Ciejk E, Thorner J (1979) Recovery of *S. cerevisiae* a cells from G1 arrest by α factor pheromone requires endopeptidase action. *Cell* 18: 623-35.

[27] Minina S, Reichman-Fried M, Raz E (2007) Control of receptor internalization, signaling level, and precise arrival at the target in guided cell migration. *Curr Biol* 17: 1164-1172.

[28] Li L, Nrrelykke SF, Cox EC (2008) Persistent Cell Motion in the Absence of External Signals: A Search Strategy for Eukaryotic Cells *PLoS One* 3: e2093.

[29] Thar R, Kühl (2003) Bacteria are not too small for spatial sensing of chemical gradients: an experimental evidence. *Proc Natl Acad Sci USA* 100: 5748-5753.

[30] Meinhardt H (1999) Orientation of chemotactic cells and growth cones: models and mechanisms. *J Cell Sci* 112: 2867-2874.

[31] Skupsky R, Losert W, Nossal RJ (2005) Distinguishing modes of eukaryotic gradient sensing. *Biophys J* 89: 2806-2823.

[32] Narang A (2006) Spontaneous polarization in eukaryotic gradient sensing: a mathematical model based on mutual inhibition of frontness and backness pathways. *J Theor Biol* 240: 538-553.

[33] Levine H, Kessler DA, Rappel WJ (2006) Directional sensing in eukaryotic chemotaxis: a balanced inactivation model. *Proc Natl Acad Sci USA* 103: 9761-9766.

[34] Krishnan J, Iglesias PA (2007) Receptor-mediated and intrinsic polarization and their interaction in chemotaxing cells. *Biophys J* 92: 816-830.

[35] Onsum M, Rao CV (2007) A mathematical model for neutrophil gradient sensing and polarization. *PLoS Comput Biol* 3: e36.

[36] Otsuji M, Ishihara S, Co C, Kaibuchi K, Mochizuki A, Kuroda S (2007) A mass conserved reaction-diffusion system captures properties of cell polarity. *PLoS Comput Biol* 3: e108.

- [37] Dawes AT, Bard Ermentrout G, Cytrynbaum EN, Edelstein-Keshet L (2006) Actin filament branching and protrusion velocity in a simple 1D model of a motile cell. *J Theor Biol* 242: 265-279.
- [38] Dawes AT, Edelstein-Keshet L (2007) Phosphoinositides and Rho proteins spatially regulate actin polymerization to initiate and maintain directed movement in a one-dimensional model of a motile cell. *Biophys J* 92: 744-768.
- [39] Plisson E, Lee KJ, Goldstein RE, Franke J, Kessin RH, Cox EC (1997) Selection for spiral waves in the social amoebae *Dictyostelium*. *Proc Natl Acad Sci USA* 94: 13719-13723.
- [40] Goodhill GJ, Urbach JS (1999) Theoretical analysis of gradient detection by growth cones. *J Neurobiol* 41: 230-241.
- [41] Wylie CS, Levine H, Kessler DA (2006) Fluctuation-induced instabilities in front propagation up a comoving reaction gradient in two dimensions. *Phys Rev E Stat Nonlin Soft Matter Phys* 74: 016119.
- [42] Iglesias PA, Devreotes PN (2008) Navigating through models of chemotaxis. *Curr Opin Cell Biol* 20: 35-40.
- [43] Andrews BW, Iglesias PA (2007) An information-theoretic characterization of the optimal gradient sensing response of cells. *PLoS Comput Biol* 3: e153.
- [44] Samadani A, Mettetal J, van Oudenaarden A (2006) Cellular asymmetry and individuality in directional sensing. *Proc Natl Acad Sci USA* 103: 11549-11554.
- [45] Skupsky R, McCann C, Nossal R, Losert W (2007) Bias in the gradient-sensing response of chemotactic cells. *J Theor Biol* 247: 242-258.

Accuracy of direct gradient sensing by single cells

Supplementary information

Robert G. Endres^{1,2} and Ned S. Wingreen¹

¹*Department of Molecular Biology,*

Princeton University,

Princeton, NJ 08544-1014.

²*Division of Molecular Biosciences,*

and Centre for Integrated Systems Biology,

Imperial College, London SW7 2AZ,

United Kingdom.

I. ACCURACY OF CONCENTRATION AND GRADIENT SENSING BY A PERFECTLY ABSORBING SPHERE

Consider as a measurement device a sphere of radius a that is a perfect absorber for a certain dissolved chemical. The device can be used to measure both the local concentration and the local gradient of the chemical by sensing the chemical current density \vec{j} impinging on the surface of the sphere. At steady-state, for the case of a uniform particle concentration c_0 far away from the absorbing sphere, the average current is $J = 4\pi a D c_0$, where D is the particle diffusion constant [1]. Since the average number of particles $N = 4\pi D a c_0 T$ absorbed in time T is Poisson distributed, *i.e.* $\langle(\delta N)^2\rangle = \langle N \rangle$, the perfectly absorbing sphere has a concentration-measurement uncertainty of

$$\frac{\langle(\delta c)^2\rangle}{c^2} = \frac{\langle(\delta N)^2\rangle}{\langle N \rangle^2} = \frac{1}{4\pi D a c T}. \quad (11)$$

The perfectly absorbing sphere can also be used to measure the local gradient of the chemical. To calculate the current density \vec{j} in this case, we utilize a standard analogy to electrostatics. In electrostatics the potential ϕ and electric field \vec{E} in a charge-free environment are determined by Laplace's equation, $\nabla^2 \phi = 0$, and $\vec{E} = -\vec{\nabla} \phi$, respectively. As a result, the surface-charge density σ_{charge} on a conducting sphere (boundary condition $\phi = 0$ at $r = a$) placed in an electric field of magnitude E_z in the z -direction with an additional constant potential ϕ far away from the sphere is given by the superposition [2]

$$\sigma_{\text{charge}} = -\frac{1}{4\pi} \frac{\partial \phi}{\partial r} \Big|_{r=a} = -\frac{1}{4\pi} \left(\frac{\phi}{a} - 3E_z \cos \theta \right) \quad (12)$$

in Gaussian units, where θ is the polar angle measured with respect to the z axis. In the case of a chemical-absorbing sphere, the chemical concentration c and the current density \vec{j} obey equations analogous to the ones governing the potential ϕ and electric field \vec{E} in electrostatics. Specifically, the spatial dependence of the concentration c follows from the diffusion equation at steady-state, $\nabla^2 c = 0$, while the current density is given by $\vec{j} = -D \vec{\nabla} c$. Exploiting the result from electrostatics, Eq. 12, the average current density impinging on the perfectly absorbing sphere (boundary condition $c = 0$ at $r = a$) in a background gradient $c_z = \partial c / \partial z$ in the z -direction is given by

$$j(\theta) = \frac{D c_0}{a} + 3 D c_z \cos \theta. \quad (13)$$

This expression can be generalized to a gradient $\vec{\nabla}c$ in an arbitrary direction \vec{r} via

$$j(\theta, \phi) = \frac{Dc_0}{a} + 3D\vec{\nabla}c \cdot \vec{e}(\theta, \phi), \quad (14)$$

where $\vec{e}(\theta, \phi) = (\cos \phi \sin \theta, \sin \phi \sin \theta, \cos \theta)$.

To best estimate the chemical gradient from an observed density of particles absorbed at the surface of the sphere during time T , we fit the observed density $\sigma_T^{\text{obs}} = \sum_{i=1}^N \delta(\vec{r} - \vec{r}_i)$, where N is the total number of absorbed particles, to the expected density $j(\theta, \phi)T$ from Eq. 14. The best fit is obtained by minimizing the error between the observed density and the expected density

$$\text{Error} = \int [\sigma_T^{\text{obs}} - C - \sum_{m=-1,0,1} G_m Y_{l=1}^m(\theta, \phi)]^2 dA, \quad (15)$$

where C and G_m are the parameters to be determined. Note that in Eq. 15 we write the expected contribution from the gradient in terms of the spherical harmonics $Y_{l=1}^m(\theta, \phi)$: $Y_1^{-1} = \sqrt{\frac{3}{8\pi}} \sin \theta e^{-i\phi}$, $Y_1^0 = \sqrt{\frac{3}{4\pi}} \cos \theta$, $Y_1^1 = -\sqrt{\frac{3}{8\pi}} \sin \theta e^{i\phi}$. Minimizing the error as a function of the parameters C and G_m ($m = -1, 0, 1$) is achieved by setting $\partial \text{Error} / \partial C = 0$ and $\partial \text{Error} / \partial G_m = 0$, which results in the best-fit values

$$C = \frac{\int \sigma_T^{\text{obs}} dA}{\int dA} = \frac{\int \sigma_T^{\text{obs}} dA}{4\pi a^2} \quad (16)$$

$$G_{-1} = \frac{\int \sigma_T^{\text{obs}} Y_1^{-1}(\theta, \phi) dA}{\int |Y_1^{-1}(\theta, \phi)|^2 dA} = \frac{\sqrt{\frac{3}{2\pi}} \int \sigma_T^{\text{obs}} \sin \theta e^{-i\phi} dA}{a^2} \quad (17)$$

$$G_0 = \frac{\int \sigma_T^{\text{obs}} Y_1^0(\theta, \phi) dA}{\int |Y_1^0(\theta, \phi)|^2 dA} = \frac{\frac{1}{2} \sqrt{\frac{3}{\pi}} \int \sigma_T^{\text{obs}} \cos \theta dA}{a^2} \quad (18)$$

$$G_1 = \frac{\int \sigma_T^{\text{obs}} Y_1^1(\theta, \phi) dA}{\int |Y_1^1(\theta, \phi)|^2 dA} = \frac{-\sqrt{\frac{3}{2\pi}} \int \sigma_T^{\text{obs}} \sin \theta e^{i\phi} dA}{a^2} \quad (19)$$

and therefore the following best estimates for the background concentration and the individual gradient components:

$$c_0 = \frac{aC}{DT} \quad (20)$$

$$c_x = \frac{1}{6DT} \sqrt{\frac{3}{2\pi}} (G_{-1} - G_1) \quad (21)$$

$$c_y = \frac{-i}{6DT} \sqrt{\frac{3}{2\pi}} (G_1 + G_{-1}) \quad (22)$$

$$c_z = \frac{1}{6DT} \sqrt{\frac{3}{\pi}} G_0. \quad (23)$$

Since $c_{x,y,z}$ are estimates of the independent, orthogonal components of the gradient, without loss of generality, we consider only the gradient estimate in the z -direction and generalize to an arbitrary gradient later. From Eq. 23, the best estimate for the gradient in the z -direction after absorption of particles for a time T is given by

$$c_z = \frac{\int \sigma_T^{\text{obs}} \cos \theta dA}{4\pi Da^2 T} = \frac{\sum_{i=1}^N \cos \theta_i}{4\pi Da^2 T}. \quad (24)$$

We are ultimately interested in the uncertainty (accuracy) of the gradient measurement by the absorbing sphere, which is given by the variance

$$\langle (\delta c_z)^2 \rangle = \langle c_z^2 \rangle - \langle c_z \rangle^2 \quad (25)$$

$$= \frac{\langle \sum_{i=1}^N \cos^2 \theta_i \rangle + \langle \sum_{i=1}^N \sum_{i \neq j} \cos \theta_i \cos \theta_j \rangle}{(4\pi Da^2 T)^2} - \frac{\langle \sum_{i=1}^N \cos \theta_i \rangle^2}{(4\pi Da^2 T)^2} \quad (26)$$

$$= \frac{\langle \sum_{i=1}^N \cos^2 \theta_i \rangle}{(4\pi Da^2 T)^2} = \frac{\langle N \rangle \langle \cos^2 \theta \rangle}{(4\pi Da^2 T)^2} = \frac{c_0}{12\pi Da^3 T}. \quad (27)$$

Deriving Eq. 27 made use of the independence of the particles to factorize the expectation value $\langle \sum_{i=1}^N \sum_{i \neq j} \cos \theta_i \cos \theta_j \rangle = \langle N(N-1) \rangle \langle \cos \theta \rangle^2 = \langle N \rangle^2 \langle \cos \theta \rangle^2$, since N is Poisson distributed. The last step is exact. We also used $\langle N \rangle = 4\pi Da c_0 T$, as well as $\langle \cos^2 \theta \rangle = 1/3$. The latter relation applied to absorbed particles holds even in the presence of a gradient in the z direction since the average $\langle \cos^3 \theta \rangle$ is zero.

Since the gradient may point in an arbitrary direction, the total uncertainty of the gradient, normalized by c_0/a , is given by

$$\frac{\langle (\delta c_{\vec{r}})^2 \rangle}{(c_0/a)^2} = \frac{3\langle (\delta c_z)^2 \rangle}{(c_0/a)^2} = \frac{1}{4\pi Da c_0 T}, \quad (28)$$

with the factor of 3 arising because each component of the gradient contributes independently to the total uncertainty. This result for the uncertainty in gradient sensing is independent of the magnitude of the actual gradient present (including the case when no gradient is present). Interestingly, the result is identical to the uncertainty in measuring the concentration by the same perfectly absorbing sphere (*cf.* Eq. 11).

Special case: absorbing sphere with two polar measurement patches

We consider a special case in which a whole sphere of radius a is absorbing, but only two small circular patches of radius s ($\ll a$) opposite to each other on the sphere measure the

number of absorbed particles. We start with the analogues of Eqs. 18 and 24 for the estimated gradient in the z -direction

$$G_0 = \frac{\int \sigma_T^{\text{obs}} \cos \theta dA}{\sqrt{3\pi}s^2} \quad (29)$$

$$c_z = \frac{G_0}{2\sqrt{3\pi}DT} = \frac{\int \sigma_T^{\text{obs}} \cos \theta dA}{6\pi Ds^2T} = \frac{N_1 - N_2}{6\pi Ds^2T}, \quad (30)$$

where we have used $\cos \theta \approx 1$ for patch 1 and $\cos \theta \approx -1$ for patch 2. The variance is given by

$$\langle (\delta c_z)^2 \rangle = \langle c_z^2 \rangle - \langle c_z \rangle^2 \quad (31)$$

$$= \frac{\langle (N_1 - N_2)^2 \rangle}{(6\pi Ds^2T)^2} - \frac{\langle (N_1 - N_2) \rangle^2}{(6\pi Ds^2T)^2} \quad (32)$$

$$= \frac{\langle (\delta N_1)^2 \rangle + \langle (\delta N_2)^2 \rangle}{(6\pi Ds^2T)^2} \quad (33)$$

$$= \frac{c_0}{18\pi Ds^2aT} \quad (34)$$

where we have used $\langle \delta N_i^2 \rangle = \langle N_i^2 \rangle - \langle N_i \rangle^2 = \langle N_i \rangle$ ($i = 1, 2$) for a Poisson process, as well as $\langle N_1 \rangle = \pi s^2 DT(c_0 + \langle c_z \rangle a)/a$ and $\langle N_2 \rangle = \pi s^2 DT(c_0 - \langle c_z \rangle a)/a$. From this we obtain the normalized uncertainty of the gradient in the z direction

$$\frac{\langle (\delta c_z)^2 \rangle}{(c_0/a)^2} = \frac{1}{12\pi D a c_0 T} \cdot \frac{2a^2}{3s^2}, \quad (35)$$

i.e. $2a^2/(3s^2)$ times the uncertainty in the gradient using the whole sphere. Hence, the smaller the patch size s , the larger in the uncertainty of the gradient measurement.

II. ACCURACY OF GRADIENT SENSING BY A PERFECTLY MONITORING SPHERE

Berg and Purcell considered a “perfect instrument” for measuring the concentration of a certain dissolved chemical, namely a virtual sphere of radius a that could exactly count the number of diffusing chemical molecules inside its volume [1]. They showed that such an instrument, making measurements for a time T , could estimate a concentration with an uncertainty

$$\frac{\langle (\delta c)^2 \rangle}{c^2} = \frac{3}{5\pi D a c T}. \quad (36)$$

We note that the “perfect instrument” is actually inferior by a factor $12/5$ in variance to the perfectly absorbing sphere for concentration measurement (Eq. 11) because the absorbing

sphere removes particles from the environment, and hence does not measure the same particle more than once.

We extend Berg and Purcell's analysis of the perfect instrument to include gradient sensing by assuming that the virtual sphere also measures the positions of all particles in its volume. As in the previous section, we derive a best estimate for the gradient and the variance of this best estimate to find the uncertainty of the gradient determination. We start by fitting a gradient model $c = c_0 + \vec{r} \cdot \vec{c}_r$ to the observed time-averaged number density $\frac{1}{T} \int dt \rho_{\text{obs}}(t) = \frac{1}{T} \int dt \sum_{i=1}^N \delta(\vec{r} - \vec{r}(t))$, obtained by measuring the exact positions of the particles inside the volume of the sphere for a time T . Specifically, we minimize the error

$$\text{Error} = \int \left(\frac{1}{T} \int \rho_{\text{obs}}(t) dt - c_0 - \vec{r} \cdot \vec{c}_r \right)^2 dV. \quad (37)$$

As before we focus on one component of the gradient, namely the gradient in the z -direction c_z . By setting $\partial \text{Error} / \partial c_z = 0$, we obtain as a best estimate for the z gradient

$$c_z = \frac{\frac{1}{T} \int dt \int dV z \rho_{\text{obs}}(t)}{\int dV z^2}. \quad (38)$$

We are interested in the variance of this estimated gradient

$$\langle (\delta c_z)^2 \rangle = \langle c_z^2 \rangle - \langle c_z \rangle^2 \quad (39)$$

$$= \left(\frac{15}{4\pi a^5} \right)^2 \cdot \frac{1}{T^2} \left[\left\langle \left(\int dt \int dV z \rho_{\text{obs}}(t) \right)^2 \right\rangle - \left\langle \left(\int dt \int dV z \rho_{\text{obs}}(t) \right) \right\rangle^2 \right] \quad (40)$$

$$= \left(\frac{15}{4\pi a^5} \right)^2 \left[\langle m_{z,T}^2 \rangle - \langle m_{z,T} \rangle^2 \right], \quad (41)$$

where we have used $\int dV z^2 = 4\pi a^5 / 15$ and we have defined

$$\langle m_{z,T}^2 \rangle = \frac{1}{T^2} \left\langle \left(\int dt \int dV z \rho_{\text{obs}}(t) \right)^2 \right\rangle = \frac{1}{T^2} \int_0^T dt \int_0^T dt' \langle m_z(t) m_z(t') \rangle, \quad (42)$$

$$\langle m_{z,T} \rangle = \frac{1}{T} \left\langle \left(\int dt \int dV z \rho_{\text{obs}}(t) \right) \right\rangle = \frac{1}{T} \int_0^T dt \langle m_z(t) \rangle. \quad (43)$$

The quantity $m_z(t)$ is the total of the z coordinates of all the particles inside the sphere at time t . To calculate $m_z(t)$, consider the sphere imbedded inside a much larger volume containing a total of M particles. This results in $m_z(t) = \sum_{i=1}^M z_i(t)$, where z_i is the z -coordinate of particle i if this particle is inside the sphere and zero if it is outside. If $N(t)$ is the number of particles inside the sphere at time t , then on average there will be

$\langle N \rangle = \frac{4}{3}\pi a^3 c_0$ particles inside the sphere. The auto-correlation function $\langle m_z(t)m_z(t') \rangle$ of particles inside the sphere at time t and time t' can consequently be calculated

$$\langle m_z(t)m_z(t') \rangle = \left\langle \sum_{i=1}^M \sum_{j=1}^M z_i(t)z_j(t') \right\rangle \quad (44)$$

$$= \left\langle \sum_{i=1}^M z_i(t)z_i(t') \right\rangle + \left\langle \sum_{i=1}^M z_i(t) \right\rangle \cdot \left\langle \sum_{j \neq i}^M z_j(t') \right\rangle \quad (45)$$

$$= \langle N \rangle \langle z(t)z(t') \rangle + \langle N \rangle^2 \langle z(t) \rangle^2 \quad (46)$$

$$= \frac{4}{3}\pi a^3 c_0 u(t-t') + \langle m_z(t) \rangle^2, \quad (47)$$

where we defined $u(t-t') = \langle z(t)z(t') \rangle$. For Eq. 46 we used that $\langle \sum_{j \neq i}^M z_j(t') \rangle \approx \langle \sum_{j=1}^M z_j(t') \rangle$, which is exact in the thermodynamic limit of the large embedding volume and large M . Furthermore, since $N(t)$ and $z(t)$ are independent, the factorization of the expectation values is exact as well. Plugging Eqs. 47 and 43 into Eq. 41 results in

$$\langle (\delta c_z)^2 \rangle = \frac{75c_0}{4\pi a^7 T^2} \int_0^T dt \int_0^T dt' u_0(t-t'), \quad (48)$$

where the second term in Eq. 47 cancels Eq. 43.

By introducing a correlation time $\tau_z = 1/a^2 \cdot \int_0^\infty d\tau u(\tau)$ for $z(t)$, the double time integral in Eq. 48 can be simplified, provided time T is much larger than τ_z . Using time-reversal symmetry $u(\tau) = u(-\tau)$ for equilibrium diffusion (small gradients), the variance transforms into

$$\langle (\delta c_z)^2 \rangle = \frac{75c_0 \tau_z}{2\pi a^5 T}. \quad (49)$$

The remaining task is to calculate τ_z , the probability that a particle with coordinate z inside the sphere at time $t=0$ is still (or again) inside the sphere at a later time τ . Since the chemical concentration consists of a constant background concentration plus a gradient, we first consider the constant background and later consider the additional gradient.

Based on the solution of the diffusion equation, if a unit amount of chemical is released at point \vec{r}' , the concentration at point \vec{r} at a later time τ is given by

$$f(|\vec{r} - \vec{r}'|, \tau) = \frac{\exp\left(-\frac{|\vec{r} - \vec{r}'|^2}{4D\tau}\right)}{(4\pi D\tau)^{\frac{3}{2}}}. \quad (50)$$

Using the result for the time integral in Ref. [1]

$$\int_0^\infty d\tau f(|\vec{r} - \vec{r}'|, \tau) = \frac{1}{4\pi D |\vec{r} - \vec{r}'|}, \quad (51)$$

the correlation time τ_z can be expressed as a volume integral over the sphere (the initial coordinate \vec{r}' is uniform in the sphere because we assume a uniform background chemical concentration)

$$\tau_z = \frac{1}{\frac{4}{3}\pi a^3} \int_0^\infty d\tau \int dV z \int dV' z' f(|\vec{r} - \vec{r}'|, \tau) \quad (52)$$

$$= \frac{3}{16\pi^2 Da^3} \int dV z \int dV' \frac{z'}{|\vec{r} - \vec{r}'|} = \frac{3}{16\pi^2 Da^3} \int dV z \psi(r, \theta), \quad (53)$$

where $r = |\vec{r}|$. The function $\psi(r, \theta)$ is analogous to the potential of a charge density that is rotationally symmetric around the z -axis in electrostatics, *i.e.* $\rho(z') = z' = \rho(r', \theta') = r' \cos \theta'$ for $r' \leq a$ and $\rho(r') = 0$ for $r' > a$. To solve the integral in Eq. 53, we perform a multipole expansion of the potential

$$\psi(r, \theta) = \int dV' \frac{r' \cos \theta'}{|\vec{r} - \vec{r}'|} \quad (54)$$

in terms of Legendre polynomials $P_l(\cos \theta)$, exploiting the rotational symmetry about the z axis [2]. One needs to differentiate two cases:

Case I ($r' < r \leq a$):

$$\psi_>(r, \theta) = \sum_{l=0}^{\infty} \left(\frac{Q_l}{r^{l+1}} \right) P_l(\cos \theta), \quad (55)$$

where the exterior multipole moments are given by $Q_l = \int dV' \rho(\vec{r}') r'^l P_l(\cos \theta')$ with $\rho(\vec{r}') = r' \cos \theta'$. Performing the integral, only the dipole moment survives

$$Q_1 = \frac{4\pi r^5}{15}, \quad (56)$$

yielding

$$\psi_>(r, \theta) = \frac{4\pi r^3}{15} \cos \theta. \quad (57)$$

Case II ($r < r' \leq a$):

$$\psi_<(r, \theta) = \sum_{l=0}^{\infty} I_l r^l P_l(\cos \theta), \quad (58)$$

where the interior multipole moments are defined as $I_l = \int dV' \frac{\rho(\vec{r}')}{r'^{l+1}} P_l(\cos \theta')$ and, again, only the dipole moment survives

$$I_1 = \frac{2\pi(a^2 - r^2)}{3}, \quad (59)$$

yielding

$$\psi_<(r, \theta) = \frac{2\pi r(a^2 - r^2)}{3} \cos \theta. \quad (60)$$

Using these expressions for the potential, the remaining integral in Eq. 53 can be performed by summing up the two contributions to the potential $\psi(r, \theta) = \psi_<(r, \theta) + \psi_>(r, \theta)$

$$\tau_z = \frac{2\pi}{\frac{16}{3}\pi^2 Da^5} \int_0^a dr r^3 \int_0^\pi d\theta \sin \theta \cos \theta [\psi_<(r, \theta) + \psi_>(r, \theta)] = \frac{2a^2}{105D}. \quad (61)$$

Now consider the contribution from an additional gradient with zero mean over the volume of the sphere. We need to integrate $\int d^3\vec{r} \dots$ over a non-uniform distribution in Eqs. 53 and 61. Since a gradient along the z -axis contributes a factor $\cos \theta$, leading to the vanishing integral $\int_0^\pi \sin \theta \cos^3 \theta d\theta = 0$, only the constant background contributes to the uncertainty in the gradient measurement.

The result for τ_z (Eq. 61) can be used in Eq. 49 to obtain the normalized uncertainty of the gradient measurement by the perfect instrument

$$\frac{\langle (\delta c_z)^2 \rangle}{(c_0/a)^2} = \frac{5}{7\pi Da c_0 T}. \quad (62)$$

Since each component of the gradient contributes independently, the total normalized uncertainty is finally

$$\frac{\langle (\delta c_{\vec{r}})^2 \rangle}{(c_0/a)^2} = \frac{15}{7\pi Da c_0 T}. \quad (63)$$

Hence, the “perfect instrument” is not only inferior to the perfectly absorbing sphere for concentration sensing by a factor of 12/5 in variance (*cf.* Eqs. 36 and 11), but is also inferior by an even larger factor of 60/7 for gradient sensing (Eq. 28).

[1] Berg HC, Purcell EM (1977) Physics of chemoreception. *Biophys J* 20: 193-219.

[2] Jackson JD (1975) *Classical Electrodynamics* (2nd Ed., Wiley, New York), Ch. 4.4.

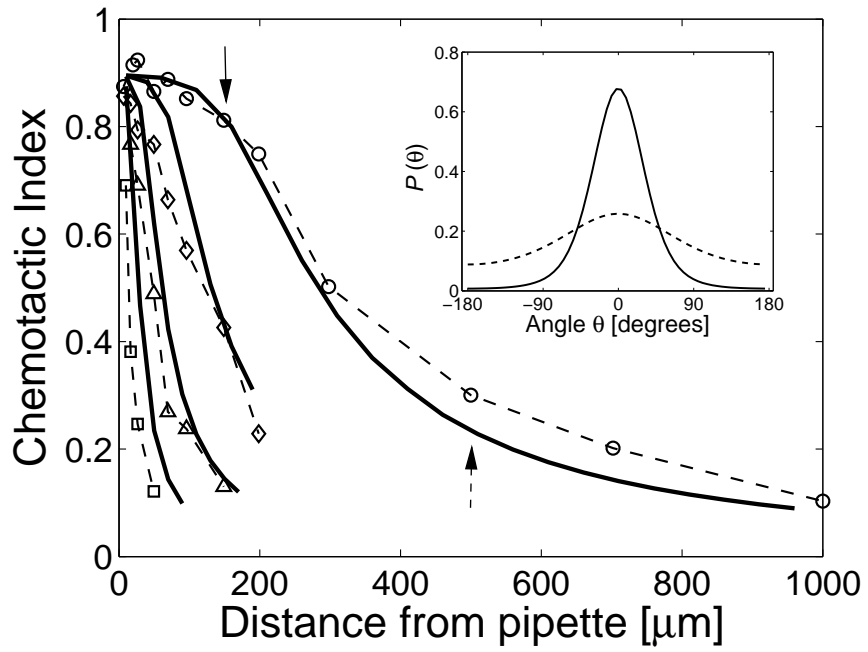


FIG. 1: Main panel is reproduced from main text Fig. 1, showing the Chemotactic Index of *Dictyostelium discoideum* cells migrating toward a pipette. Symbols correspond to four different cAMP concentrations, $0.1 \mu\text{M}$ (squares), $1 \mu\text{M}$ (triangles), $10 \mu\text{M}$ (diamonds), $100 \mu\text{M}$ (circles). Inset: predicted distributions of cell-movement directions at the two points of the $100 \mu\text{M}$ cAMP curve indicated by arrows, distances $200 \mu\text{m}$ (solid curve and arrow) and $500 \mu\text{m}$ (dashed curve and arrow) from the pipette.